

Systematic large flavor fTWA approach to interaction quenches in the Hubbard model

Alexander Osterkorn* and Stefan Kehrein

*Institute for Theoretical Physics, Georg-August-Universität Göttingen,
Friedrich-Hund-Platz 1 - 37077 Göttingen, Germany*

(Dated: July 13, 2020)

We present benchmark results for the recently introduced fermionic truncated Wigner approximation that we combine with the fermion degeneracy N as a semiclassical expansion parameter. The method is used to compute the time-evolution after an interaction quench in the two-dimensional Hubbard model starting from the noninteracting Fermi sea. Using both a numerical and a perturbative approach we show that the semiclassical dynamics is valid at least up to the prethermalization regime.

I. INTRODUCTION

The dynamics of quantum systems out-of-equilibrium¹ is a very active field of research that offers a lot of open fundamental questions as well as many perspectives for technological applications. The research is strongly driven by better and better possibilities to realize quantum mechanical model systems with ultracold gas experiments² and by the advancement of time-resolved experimental techniques in solid state physics³. In the latter context layered two-dimensional strongly correlated materials like the transition metal dichalcogenides⁴ are currently moving into the center of interest. In time-resolved angle-resolved photoemission spectroscopy (trARPES), one of the main experimental techniques to unravel the microscopic structure of such materials, the response of the electronic system to the application of a strong laser pulse is measured. This in turn requires reliable theoretical simulations of such setups in order to link the experimental observations with microscopic models^{5,6}. However, theoretical simulations of the light-induced quantum dynamics in correlated systems are very challenging due to the lack of a numerical or analytical method that is valid both for a broad range of systems and over long timespans⁷. Established approaches include tensor-network based methods⁸, the non-equilibrium extension of dynamical mean-field theory (DMFT)^{9,10} as well as perturbative schemes. While the first are very powerful for one-dimensional quantum systems, their usefulness is very restricted for time-dependent problems in 2d. Non-equilibrium DMFT is believed to work well for three-dimensional materials, its reliability in only two spatial dimensions is not clear because of the approximation of the lattice as high dimensional and the lack of systematic error bounds. Perturbative approaches are applicable to many systems but are limited to weak interactions, can suffer from secular terms¹¹ and may not be able to treat explicitly time-dependent Hamiltonians.

In theoretical quantum optics semiclassical descriptions have shown to be useful to simulate the dynamics of interacting bosons^{12,13}. Unfortunately much less experience with semiclassics for fermions exists and only recently some method development in this direction was

reported^{14,15}. These developments naturally raise the question which quantum effects are captured by a semiclassical treatment of lattice fermions and if such an approach is also useful in 2d. In this text we therefore adopt one of these recent developments, the fermionic truncated Wigner approximation (fTWA) and apply it to the well-understood problem of the interaction quench in the Hubbard model, which we consider on a two-dimensional lattice. After a review of the method, we combine it with an explicit semiclassical expansion parameter and present perturbative as well as numerical results in order to shed some light on these questions.

II. SEMICLASSICAL QUANTUM DYNAMICS

A. General framework

The concept of semiclassical dynamics encompasses a number of approaches that replace a full quantum mechanical description of a physical system by a classical description and allow to incorporate quantum effects in a controlled way. A typical way to construct such theories is a formal expansion of the quantum theory in \hbar . The leading order contribution at $\hbar \rightarrow 0$ yields a description in terms of classical variables. In particular, quantum Hamiltonians are converted into classical Hamiltonian systems. An intuitive understanding of this stems from the trivialization of commutator relations like $[\hat{q}, \hat{p}] = i\hbar$ in this limit.

Many quantum systems contain a natural expansion parameter that can be used to define an "effective \hbar ". Among the most prominent examples are large-spin and large- N expansions^{16,17} as well as expansions in the mode occupation of Bose-Einstein condensates¹⁸. The resulting classical theory is often interpretable as a mean-field description of the original quantum theory. In the case of interacting bosons, for instance, the leading order classical description is given by the Gross-Pitaevskii equation, which is as well obtained from a Hartree-Fock mean-field description of the interaction term.

Arguably the most prominent approach to add quantum corrections in a systematic manner is the truncated Wigner approximation (TWA). Working in the phase

space formulation of quantum mechanics, it can be obtained from a systematic expansion of the von Neumann equation in \hbar and a subsequent truncation to order \hbar^{19} . Alternatively, a derivation from the path integral representation of the Keldysh formalism is possible¹³.

The idea at the heart of TWA is that of an effective Liouville dynamics. Using a set $\underline{\rho}$ of phase space variables that fully characterize the physical system, like coordinate and momentum, spin components or bosonic modes, states are described in terms of their Wigner quasi-probability distributions $W(\underline{\rho})$. Their time-evolution in turn is governed by the flow generated from the Hamiltonian H_{class} that corresponds to the zeroth order classical description

$$i\partial_t W(\underline{\rho}) \simeq \{H_{\text{class}}(\underline{\rho}), W(\underline{\rho})\}. \quad (1)$$

This effective Liouville equation gives rise to a prescription for the evaluation of operator expectation values via the statistical averaging over trajectories in phase space

$$\langle \hat{O}(t) \rangle \simeq \int d\underline{\rho} W(\underline{\rho}) O_{\text{W}}(\underline{\rho}(t)), \quad (2)$$

Here, $\underline{\rho}(t)$ is time-evolved according to the Hamiltonian equations of motion for H_{class} and O_{W} denotes the classical analogue of the quantum mechanical operator \hat{O} , i.e. its Weyl symbol¹⁹.

B. Semiclassics for fermions

While the TWA as described above was successfully applied to bosonic systems, it was only recently extended to fermionic degrees of freedom¹⁵. The extension is called fermionic TWA (fTWA) and defines a set of phase space coordinates by making use of the $so(2n)$ commutator structure of the fermionic bilinears $\hat{\rho}_{\alpha\beta} = c_{\alpha}^{\dagger}c_{\beta} - \frac{1}{2}\delta_{\alpha\beta}$ and $\hat{\tau}_{\alpha\beta} = c_{\alpha}c_{\beta}$. fTWA was used to study the thermalization and echo dynamics in SYK models^{15,20} as well as the non-equilibrium dynamics in disordered Hubbard models²¹. It is worth mentioning that a very similar method was proposed even earlier in a different context under the name "stochastic mean-field approach"¹⁴.

Within fTWA the operators $\hat{\rho}_{\alpha\beta}$ and $\hat{\tau}_{\alpha\beta}$ are replaced by their associated classical phase space variables $\rho_{\alpha\beta}$ and $\tau_{\alpha\beta}$, i. e. their Weyl symbol in the context of the phase space formulation of quantum mechanics. The semiclassical time-evolution equations are derived using a mean-field decoupling of the interaction term in the fermionic many-body Hamiltonian. For the application to the Hubbard model in this text only the operators $\hat{\rho}_{\alpha\beta}$ with an index set $\alpha = i\sigma$, where i denotes the lattice site i and σ is a spin index, need to be considered.

The Wigner function is modelled within fTWA as a Gaussian distribution with means and connected covariances determined from the respective values of the quan-

tum mechanical initial state:

$$\begin{aligned} \langle \rho_{i\sigma,j\sigma} \rangle_W &\stackrel{!}{=} \langle \hat{\rho}_{i\sigma,j\sigma} \rangle_{\text{QM}}, \\ \langle \rho_{i\sigma,j\sigma}^* \rho_{k\tau,l\tau} \rangle_W^c &\stackrel{!}{=} \frac{1}{2} \left\langle \left\{ \hat{\rho}_{i\sigma,j\sigma}^{\dagger}, \hat{\rho}_{k\tau,l\tau} \right\} \right\rangle_{\text{QM}}^c \end{aligned} \quad (3)$$

C. Large- N as a semiclassical limit for lattice fermions

Despite the fact that fTWA often yields good agreement with exact calculations on short and intermediate time scales it is essentially an uncontrolled approximation. This is a consequence of the lack of a natural semiclassical expansion parameter for fermions, since in contrast to bosons occupation numbers are bounded. One possibility to systematically improve the validity of the method is to tune the range of the fermionic interactions²¹ from short-range up to very long-range.

In this text we want to adopt a large- N setup instead that keeps the short-rangedness of the interactions but increases the dimension of the local state space. Such approaches are common in equilibrium statistical physics, e. g. for frustrated magnets^{22,23}, intermediate valence systems²⁴ and correlated lattice electrons²⁵. However, only few applications of large- N techniques are known to us in the context of non-equilibrium physics²⁶. Furthermore, the experimental realization of models with N up to 10 is possible in an ultracold atom setting^{27,28}, which provides an additional motivation for the approach.

In the following we consider fermionic operators $c_{i\alpha}^{\dagger}, c_{i\alpha}$ with $\alpha = 1, \dots, N$ different spin states (flavors). Within fTWA we may now define a set of flavor-averaged phase space variables

$$\rho_{ij} = \frac{1}{N} \sum_{\alpha}^N \rho_{i\alpha,j\alpha}. \quad (4)$$

The commutation relations of the corresponding quantum mechanical operators collect an additional factor of $1/N$:

$$[\hat{\rho}_{ij}, \hat{\rho}_{mn}] = \frac{1}{N} (\delta_{jm}\hat{\rho}_{in} - \delta_{in}\hat{\rho}_{mj}) \quad (5)$$

This illustrates the semiclassical nature of the parameter N . In the limit $N \rightarrow \infty$ the commutation relations (5) are trivialized and the operators effectively become classical variables.

III. MODEL AND METHOD SETUP

In the following we study the time-evolution of the two-dimensional Fermi sea without Hubbard interaction U under a Hubbard Hamiltonian with $U > 0$:

$$H_0 = \sum_k \epsilon_k \hat{c}_k^{\dagger} \hat{c}_k \longrightarrow H = \sum_k \epsilon_k \hat{c}_k^{\dagger} \hat{c}_k + U \sum_i \hat{n}_{i\downarrow} \hat{n}_{i\uparrow}, \quad (6)$$

where $\epsilon_k = -2t_h(\cos(k_x) + \cos(k_y))$. This quench protocol was intensively studied both analytically^{29–31} and numerically^{32,33}. Among its hallmark features are the existence of a prethermalization regime at times before the thermalization dynamics dominates.

The $SU(N)$ -invariant version of the Hubbard model reads as follows³⁴:

$$\begin{aligned} \hat{H} = & t \sum_{\langle i,j \rangle} \sum_{\alpha} c_{i\alpha}^\dagger c_{j\alpha} + H.c. \\ & + \frac{U}{N} \sum_i \left(\sum_{\alpha} c_{i\alpha}^\dagger c_{i\alpha} - \frac{N}{2} \right)^2 \end{aligned} \quad (7)$$

The structure of the Hamiltonian allows for a natural representation in terms of the $\hat{\rho}$ -operators:

$$\hat{H} = N \left[t \sum_{\langle i,j \rangle} (\hat{\rho}_{ij} + \hat{\rho}_{ji}) + U \sum_i \hat{\rho}_{ii}^2 \right] \quad (8)$$

Hence, the use of flavor averaged phase space variables resolves an ambiguity in the classical representation of the interaction term which is due to the quantum mechanical identity $n_{i\alpha}^2 = n_{i\alpha}$ for fermions. At $N = 2$ the representation

$$H_{\text{int}}^{(I)} = U \sum_i \left(\rho_{i\uparrow,i\uparrow} + \frac{1}{2} \right) \left(\rho_{i\downarrow,i\downarrow} + \frac{1}{2} \right) \quad (9)$$

is quantum mechanically, but not semiclassically, equivalent to the representation derived from the $SU(N)$ invariant Hamiltonian

$$H_{\text{int}}^{(II)} = \frac{U}{2} \sum_i (\rho_{i\uparrow,i\uparrow} + \rho_{i\downarrow,i\downarrow})^2. \quad (10)$$

However, for the problem considered in this text we did not observe differing results between the two representations. In other contexts^{15,21} a specific choice of the representation has turned out to yield better numerical results than other choices.

The equations of motion for the classical ρ_{ij} can be obtained from the classical Hamiltonian formalism¹⁵ upon mean-field decoupling $\hat{\rho}_{ii}^2 \rightarrow \rho_{ii}^2$. Equivalently, they follow from the Heisenberg equations of motion corresponding to (8) in the limit $N \rightarrow \infty$.

$$i\partial_t \rho_{ij} = t \sum_{a(j)} \rho_{i,a(j)} - t \sum_{a(i)} \rho_{a(i),j} + 2U(\rho_{jj} - \rho_{ii})\rho_{ij} \quad (11)$$

The equilibrium ground state of the model with $U = 0$ is given by the N -flavor Fermi sea $|\text{FS}\rangle = \prod_{\alpha, |\vec{k}| \leq k_F} c_{\vec{k}\alpha}^\dagger |0\rangle$ whose initial data (3) in momentum space is given by

$$\begin{aligned} \langle \hat{\rho}_{kl} \rangle &= \langle \hat{\rho}_{kl}^\dagger \rangle = \delta_{k,l} \left(n_k - \frac{1}{2} \right), \\ \frac{1}{2} \langle \{\hat{\rho}_{kl}, \hat{\rho}_{sp}\} \rangle^c &= \frac{1}{2N} \delta_{kp} \delta_{ls} (n_k + n_l - 2n_k n_l) \end{aligned} \quad (12)$$

At $N \rightarrow \infty$ the Hubbard interaction U in (8) merely plays the role of a shift to the chemical potential such that non-trivial dynamics after the interaction quench can only occur at finite N .

IV. RESULTS FOR THE $SU(N)$ FTWA

A. Perturbative treatment of the e.o.m.

For small Hubbard interaction strengths $U \ll 1$ one can treat the classical equations of motion perturbatively and evaluate all expectation values with respect to the Gaussian Wigner function by hand. In order to do so it is advantageous to work with the equations in momentum space. Using the Fourier transform

$$\rho_{ij} = \sum_{kl} e^{i(kr_i - lr_j)} \rho_{kl} \quad (13)$$

one obtains

$$\begin{aligned} i\partial_t \rho_{kl} = & -(\epsilon_k - \epsilon_l) \rho_{kl} \\ & + \frac{2U}{V} \sum_{sp} (\rho_{p+s-l,p} \rho_{ks} - \rho_{p+k-s,p} \rho_{sl}). \end{aligned} \quad (14)$$

A naive perturbative expansion of these equations in U is only valid up to times $\mathcal{O}(t^2)$. In order to avoid such secular terms we switch to an interaction picture representation of the equations of motion by incorporating the free time-evolution into the variables $\tilde{\rho}_{kl} = e^{-i(\epsilon_k - \epsilon_l)t} \rho_{kl}$ where $\Delta\epsilon_{pks} = \epsilon_{p+k-s} + \epsilon_s - \epsilon_p - \epsilon_k$. This yields

$$\begin{aligned} i\partial_t \tilde{\rho}_{kl} = & \frac{2U}{V} \sum_{sp} \left[e^{i\Delta\epsilon_{p+sl}t} \tilde{\rho}_{p+s-l,p} \tilde{\rho}_{ks} \right. \\ & \left. - e^{i\Delta\epsilon_{p+k-s}t} \tilde{\rho}_{p+k-s,p} \tilde{\rho}_{sl} \right]. \end{aligned} \quad (15)$$

We may now expand the variables order by order in U

$$\tilde{\rho}_{kl} = \tilde{\rho}_{kl}^{(0)} + \tilde{\rho}_{kl}^{(1)} \cdot U + \tilde{\rho}_{kl}^{(2)} \cdot U^2 + \dots \quad (16)$$

Inserting the ansatz into (15) yields a hierarchy of equations at increasing order of U . The zeroth order contribution is constant in time, $i\partial_t \tilde{\rho}_{kl}^{(0)} = 0$. This fact allows to explicitly integrate all time dependencies in the equation for $\tilde{\rho}_{kl}^{(1)}$. In a last step all expectation values of products of $\tilde{\rho}_{kl}^{(0)}$ are evaluated using the Gaussian Wigner function. Successive application of this scheme results in an iterative procedure to solve for the dynamics to all orders of U . Formally the elastic contributions with $\Delta\epsilon_{pp'k} = 0$ need to be absorbed into the unperturbed Hamiltonian because they produce secular terms in the perturbative expansion. Details of the calculation are shown in Appendix A.

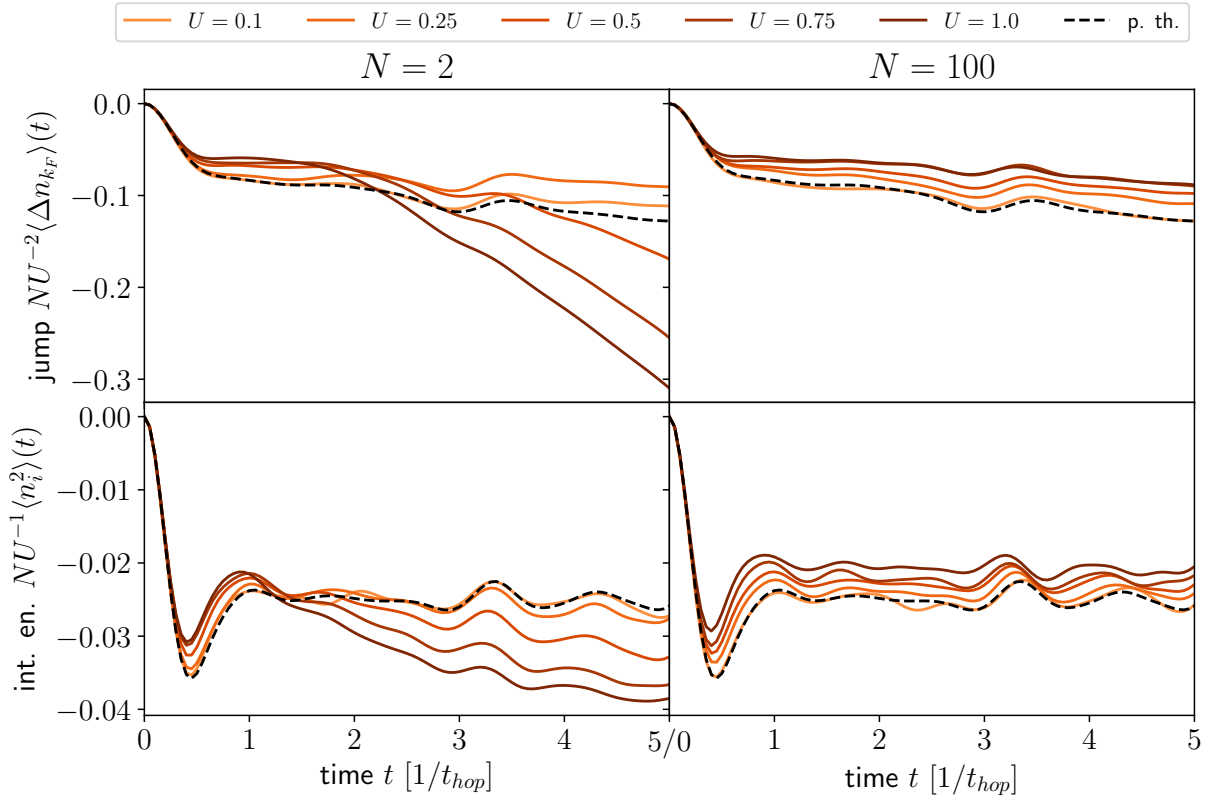


FIG. 1. Semiclassical dynamics in a 10×10 square lattice Fermi sea at quarter filling ($N = 25$ particles) after an interaction quench to weak and intermediate values of U . The two columns display results at $N = 2$ and $N = 100$. The top two panels present the jump in the momentum distribution at the Fermi energy, rescaled by a factor of N/U^2 that allows for a comparison to the result obtained from perturbation theory. In the bottom row the dynamics of the interaction energy is shown. Here the black dashed curve is calculated using the perturbative result for the occupation numbers in combination with the energy conservation during the time-evolution.

We solved the hierarchy up to order U^2 and obtained the following results:

$$\begin{aligned} \tilde{\rho}_{kl}^{(1)}(t) &= 0 \\ \tilde{\rho}_{kl}^{(2)}(t) &= -\delta_{k,l} \frac{16}{NV^2} \sum_{\substack{pp' \\ \Delta\epsilon_{pp'k} \neq 0}} \frac{\sin^2\left(\frac{\Delta\epsilon_{pp'k}}{2}t\right)}{(\Delta\epsilon_{pp'k})^2} J_{pp'k} \end{aligned} \quad (17)$$

where

$$J_{pp'k} = n_k n_{p+p'-k} (1 - n_p) (1 - n_{p'}) - n_p n_{p'} (1 - n_k) (1 - n_{p+p'-k}) \quad (18)$$

is a phase space factor. These results agree with those obtained from unitary perturbation theory²⁹.

B. Numerical results

In order to study the quench dynamics numerically we have implemented Hamilton's equations of motion using the odeint library³⁵ and the Armadillo library^{36,37}. To

avoid the accumulation of numerical errors, Welford's algorithm was used for checkpointing³⁸. We used the standard deviation of the sets of k -values with equal band energies ϵ_k to control the convergence of the simulation. We stopped sampling from the Wigner function when the relative deviations between these identical k -values became negligible.

Two characteristic quantities for the interaction quench dynamics are the jump Δn_{k_F} in the momentum distribution n_k at the Fermi energy and the interaction energy $H_{\text{int}} \sim \langle n_i^2 \rangle$. The first is directly related to the quasiparticle weight Z ²⁹ and assumes the value one for the initial Fermi-Dirac distribution. The interaction energy is, in contrast, a local quantity that is expected to equilibrate in the prethermalization regime to the equilibrium value of the post-quench Hamiltonian with respect to the final temperature. It provides a generalization of the double occupation $d(t)$ at $N = 2$. Energy conservation allows to compute the time-evolution of the interaction energy from the perturbative result (17).

Since prethermalization effects are suppressed at half filling in the 2D model³³, we consider the quarter filled case in the following. Fig. 1 shows the numerical re-

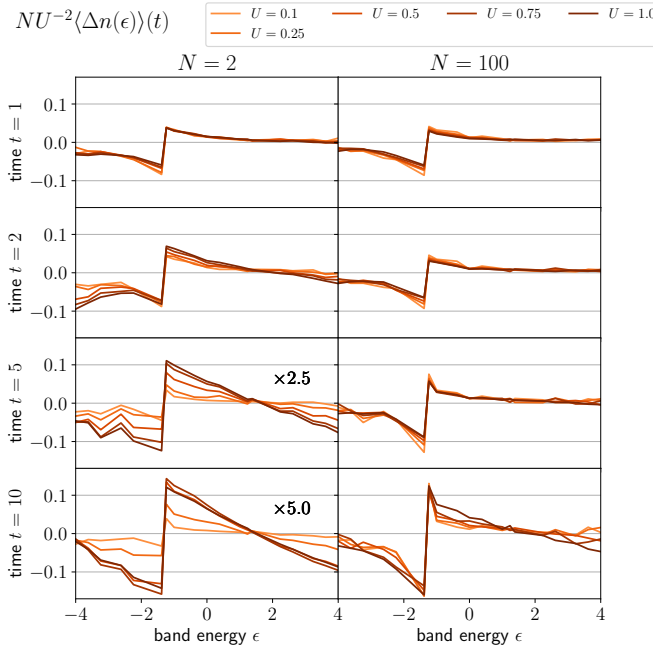


FIG. 2. Momentum distribution function as a function of the band energies ϵ for a 10×10 square lattice at quarter filling ($N = 25$ particles) after a quench to Hubbard interactions $U \leq 1$. It corresponds to the data shown in Fig. 1.

sults for Δn_{k_F} and $\langle n_i^2 \rangle$ in a 10×10 system at two fixed values of the degeneracy parameter N whereas Fig. 3 shows data for a 20×20 system at fixed U and varying N . At small U in Fig. 1 the dynamics at the Fermi edge agrees very well with the perturbative calculation. After the initial correlation build-up a prethermalization plateau is forming until, for $N = 2$, a further reduction of the jump sets in. One can observe in particular that the width of the plateau is smaller for greater values of U , whereas for $N = 100$ the prethermalization dynamics extends over a much longer timespan. The onset of this reduction with varying N can be seen in Fig. 3. Although the behaviour at $N = 2$ is in qualitative agreement with numerical calculations in infinite dimensions³², the question needs to be addressed whether it describes the true thermalization dynamics. Looking at the interaction energy the expected equilibration in the prethermal regime is found for $N \geq 100$. For smaller values of N in contrast, $\langle n_i^2 \rangle$ starts to decay even before the reduction dynamics is visible in Δn_{k_F} which is likely unphysical behavior.

To shed more light on this question we consider the momentum distribution $\langle \Delta n(\epsilon) \rangle(t) = n_\epsilon(t) - n_\epsilon(0)$, where $n_\epsilon(0) = \theta(\epsilon_F - \epsilon)$, at all single-particle energies ϵ_k shown in Figs. 2 and 4. For small N negative occupation numbers are observable close to the band edge at $\epsilon = 4$ already at early times. This becomes worse at later times and clearly indicates unphysical dynamics beyond the prethermalization regime. Hence we conclude that in the regime of weak to moderate interactions the method cap-

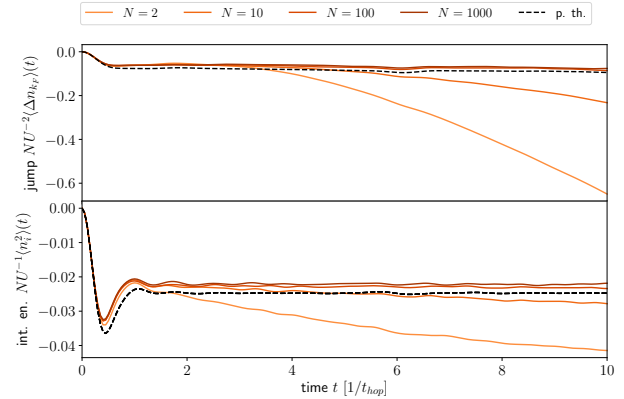


FIG. 3. Fermi surface jump and interaction energy for a 20×20 square lattice Fermi sea at quarter filling ($N = 101$ particles) after an interaction quench to $U = 0.5$ at varying N .

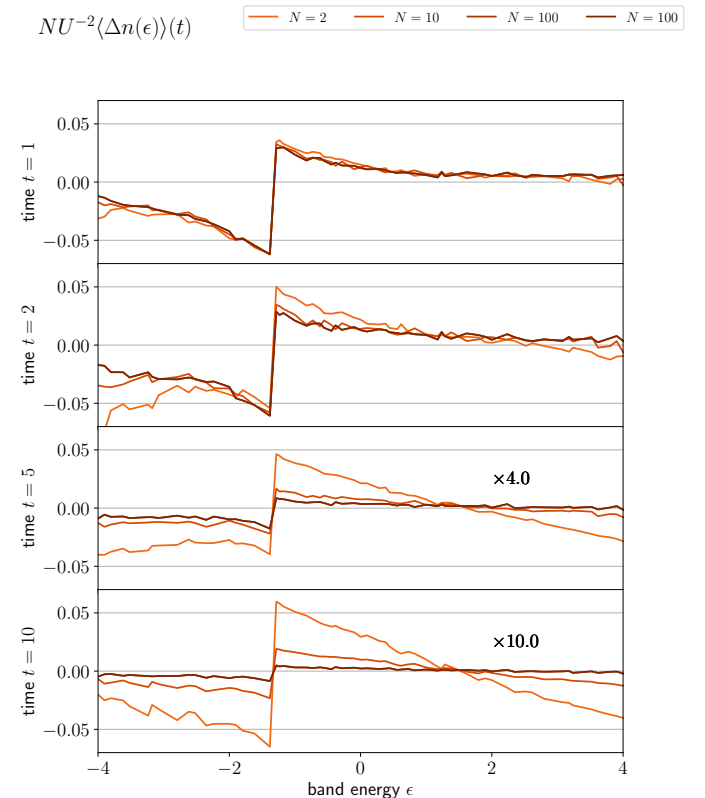


FIG. 4. Momentum distribution function as a function of the single-particle energies ϵ corresponding to the data shown in Fig. 3.

tures the dynamics at order $\frac{1}{N}$ correctly and is valid at least up to the prethermalization regime. The thermalization dynamics that follows gives a qualitatively correct picture at the Fermi energy but is not reliable due to the emergence of unphysical occupation numbers.

V. CONCLUSION

In this paper we combined the fermion degeneracy N as a semiclassical expansion parameter with the recently introduced fTWA method and used the well-understood problem of the interaction quench in the Hubbard model as a benchmarking problem. We observed that for small N the method is prone to produce unphysical results at times beyond the prethermalization regime. This agrees qualitatively with the picture that TWA describes the dynamics at linear order of the effective $\hbar \sim \frac{1}{N}$. To elucidate this issue it would be interesting to include further quantum corrections to TWA in the simulation¹⁹ or to use an optimized basis for the TWA setup. In addition, the assumption of a Gaussian Wigner function needs to be reviewed carefully, in particular with respect to the question up to which order the correlations of the initial product state are correctly described.

The computational cost of fTWA increases only polynomially in the system size, which allows the simulation of 2d lattice systems with a much larger number of sites possible than with exact diagonalization or tensor-network based approaches. Another advantage is that the Hamiltonian may in general also have an explicit time-dependence. This is relevant in the context of light-induced dynamics that is often modeled using Peierls substitution. Further work in this direction is currently in progress.

ACKNOWLEDGMENTS

We acknowledge helpful discussions with Anatoli Polkovnikov. This work was funded by the Deutsche Forschungsgemeinschaft (DFG, German Research Foundation) - 217133147/SFB 1073, project B07.

Appendix A: Details on the perturbative calculation

Since $i\partial_t \tilde{\rho}_{kl} = \mathcal{O}(U)$, $i\partial_t \tilde{\rho}_{kl}^{(0)} = 0$ follows immediately. Consequently, $\tilde{\rho}_{kl}^{(0)} = \delta_{kl} n_k(0)$. The equation of motion for the $\mathcal{O}(U)$ contribution is

$$i\partial_t \tilde{\rho}_{kl}^{(1)} = \frac{2}{V} \sum_{sp} \left[e^{i\Delta\epsilon_{psl}t} \tilde{\rho}_{p+s-l,p}^{(0)} \tilde{\rho}_{ks}^{(0)} - e^{i\Delta\epsilon_{pks}t} \tilde{\rho}_{p+k-s,p}^{(0)} \tilde{\rho}_{sl}^{(0)} \right]. \quad (\text{A1})$$

It is possible to integrate the time-dependencies explicitly using the integral

$$\mathcal{I}_1(\Delta\epsilon_{pab}) = -i \int_0^t dt' e^{i\Delta\epsilon_{pab}t'} = \begin{cases} \frac{1}{\Delta\epsilon_{pab}} (e^{i\Delta\epsilon_{pab}t} - 1) & \Delta\epsilon_{pab} \neq 0 \\ -it & \Delta\epsilon_{pab} = 0 \end{cases} \quad (\text{A2})$$

The Wigner function averages are performed manually using

$$\langle \tilde{\rho}_1^{(0)} \tilde{\rho}_2^{(0)} \rangle = \langle \tilde{\rho}_1^{(0)} \tilde{\rho}_2^{(0)} \rangle^c + \langle \tilde{\rho}_1^{(0)} \rangle \langle \tilde{\rho}_2^{(0)} \rangle \quad (\text{A3})$$

and the initial data in (3). The structure of (A1) is such that both terms cancel each other after the Wigner function averaging. Thus $\tilde{\rho}_{kl}^{(1)}(t) = 0$.

The next order $\mathcal{O}(U^2)$ already contains eight terms

$$\begin{aligned} \tilde{\rho}_{kl}^{(2)}(t) = & \frac{4}{V^2} \sum_{sps'p'} \left[\right. \\ & \mathcal{I}_2(\Delta\epsilon_{p's's}, \Delta\epsilon_{psl}) \tilde{\rho}_{(p+s-l),p}^{(0)} \tilde{\rho}_{(p'+s'-s),p'}^{(0)} \tilde{\rho}_{k,s'}^{(0)} \\ & - \mathcal{I}_2(\Delta\epsilon_{p'ks'}, \Delta\epsilon_{psl}) \tilde{\rho}_{(p+s-l),p}^{(0)} \tilde{\rho}_{(p'+k-s'),p'}^{(0)} \tilde{\rho}_{s',s}^{(0)} \\ & + \mathcal{I}_2(\Delta\epsilon_{p's'p}, \Delta\epsilon_{psl}) \tilde{\rho}_{(p'+s'-p),p'}^{(0)} \tilde{\rho}_{(p+s-l),s'}^{(0)} \tilde{\rho}_{k,s}^{(0)} \\ & - \mathcal{I}_2(\Delta\epsilon_{p'(p+s-l)s'}, \Delta\epsilon_{psl}) \tilde{\rho}_{(p'+p+s-l-s'),p'}^{(0)} \tilde{\rho}_{s',p}^{(0)} \tilde{\rho}_{k,s}^{(0)} \\ & - \mathcal{I}_2(\Delta\epsilon_{p's'l}, \Delta\epsilon_{pks}) \tilde{\rho}_{(p+k-s),p}^{(0)} \tilde{\rho}_{(p'+s'-l),p'}^{(0)} \tilde{\rho}_{s,s'}^{(0)} \\ & + \mathcal{I}_2(\Delta\epsilon_{p's's}, \Delta\epsilon_{pks}) \tilde{\rho}_{(p+k-s),p}^{(0)} \tilde{\rho}_{(p'+s-s'),p'}^{(0)} \tilde{\rho}_{s',l}^{(0)} \\ & - \mathcal{I}_2(\Delta\epsilon_{p's'p}, \Delta\epsilon_{pks}) \tilde{\rho}_{(p'+s'-p),p'}^{(0)} \tilde{\rho}_{(p+k-s),s'}^{(0)} \tilde{\rho}_{s,l}^{(0)} \\ & \left. + \mathcal{I}_2(\Delta\epsilon_{p'(p+k-s)s'}, \Delta\epsilon_{pks}) \tilde{\rho}_{(p'+p+k-s-s'),p'}^{(0)} \tilde{\rho}_{s',p}^{(0)} \tilde{\rho}_{s,l}^{(0)} \right] \end{aligned} \quad (\text{A4})$$

where

$$\mathcal{I}_2(\Delta\epsilon_{p'ab}, \Delta\epsilon_{pcd}) = - \int_0^t dt' \int_0^{t'} dt'' e^{i\Delta\epsilon_{pcd}t'} e^{i\Delta\epsilon_{p'ab}t''}. \quad (\text{A5})$$

The third moments of the Wigner function are evaluated using Wick's theorem for a Gaussian distribution

$$\begin{aligned} \langle \tilde{\rho}_1^{(0)} \tilde{\rho}_2^{(0)} \tilde{\rho}_3^{(0)} \rangle = & \langle \tilde{\rho}_1^{(0)} \rangle \langle \tilde{\rho}_2^{(0)} \tilde{\rho}_3^{(0)} \rangle^c + \langle \tilde{\rho}_2^{(0)} \rangle \langle \tilde{\rho}_1^{(0)} \tilde{\rho}_3^{(0)} \rangle^c \\ & + \langle \tilde{\rho}_3^{(0)} \rangle \langle \tilde{\rho}_1^{(0)} \tilde{\rho}_2^{(0)} \rangle^c + \langle \tilde{\rho}_1^{(0)} \rangle \langle \tilde{\rho}_2^{(0)} \rangle \langle \tilde{\rho}_3^{(0)} \rangle \end{aligned} \quad (\text{A6})$$

It turns out that after averaging over the Wigner function (A4) has the structure

$$\begin{aligned} \tilde{\rho}_{kl}^{(2)}(t) = & \delta_{kl} \frac{4}{NV^2} \sum_{pp'} J_{pp'k} \cdot \\ & \left[\mathcal{I}_2(-\Delta\epsilon_{pp'k}, \Delta\epsilon_{pp'k}) + \mathcal{I}_2(\Delta\epsilon_{pp'k}, -\Delta\epsilon_{pp'k}) \right] \end{aligned} \quad (\text{A7})$$

with

$$\begin{aligned} \mathcal{I}_2(\Delta\epsilon_{pp'k}, -\Delta\epsilon_{pp'k}) + \mathcal{I}_2(\leftrightarrow) = & \\ = & \begin{cases} -\frac{4}{(\Delta\epsilon_{pp'k})^2} \sin^2\left(\frac{\Delta\epsilon_{pp'k}}{2}t\right) & \Delta\epsilon_{pp'k} \neq 0 \\ -t^2 & \Delta\epsilon_{pp'k} = 0 \end{cases}. \end{aligned} \quad (\text{A8})$$

These calculations finally yield (17). As discussed in the main text the elastic contributions that eventually yield secular terms $\sim t^2$ may be shifted formally to the unperturbed part of the Hamiltonian.

^{*} osterkorn@theorie.physik.uni-goettingen.de

¹ A. Polkovnikov, K. Sengupta, A. Silva, and M. Vengalattore, Rev. Mod. Phys. **83**, 863 (2011), publisher: American Physical Society.

² C. Gross and I. Bloch, Science **357**, 995 (2017), publisher: American Association for the Advancement of Science Section: Review.

³ P. Dombi, Z. Ppa, J. Vogelsang, S. V. Yalunin, M. Sivis, G. Herink, S. Schfer, P. Gro, C. Ropers, and C. Lienau, Rev. Mod. Phys. **92**, 025003 (2020), publisher: American Physical Society.

⁴ S. Manzeli, D. Ovchinnikov, D. Pasquier, O. V. Yazyev, and A. Kis, Nature Reviews Materials **2**, 1 (2017), number: 8 Publisher: Nature Publishing Group.

⁵ J. K. Freericks, H. R. Krishnamurthy, and T. Pruschke, Phys. Rev. Lett. **102**, 136401 (2009).

⁶ J. K. Freericks, H. R. Krishnamurthy, M. A. Sentef, and T. P. Devereaux, Phys. Scr. **T165**, 014012 (2015).

⁷ M. Eckstein, A. Hackl, S. Kehrein, M. Kollar, M. Moeckel, P. Werner, and F. Wolf, Eur. Phys. J. Spec. Top. **180**, 217 (2009).

⁸ S. Paeckel, T. Khler, A. Swoboda, S. R. Manmana, U. Schollwck, and C. Hubig, Annals of Physics **411**, 167998 (2019).

⁹ J. K. Freericks, V. M. Turkowski, and V. Zlati, Phys. Rev. Lett. **97**, 266408 (2006), publisher: American Physical Society.

¹⁰ H. Aoki, N. Tsuji, M. Eckstein, M. Kollar, T. Oka, and P. Werner, Rev. Mod. Phys. **86**, 779 (2014), publisher: American Physical Society.

¹¹ A. Hackl and S. Kehrein, Phys. Rev. B **78**, 092303 (2008), publisher: American Physical Society.

¹² A. Sinatra, C. Lobo, and Y. Castin, J. Phys. B: At. Mol. Opt. Phys. **35**, 3599 (2002), publisher: IOP Publishing.

¹³ A. Polkovnikov, Phys. Rev. A **68**, 053604 (2003).

¹⁴ D. Lacroix, S. Hermanns, C. M. Hinz, and M. Bonitz, Phys. Rev. B **90**, 125112 (2014).

¹⁵ S. Davidson, D. Sels, and A. Polkovnikov, Annals of Physics **384**, 128 (2017).

¹⁶ L. G. Yaffe, Rev. Mod. Phys. **54**, 407 (1982).

¹⁷ N. E. Bickers, Rev. Mod. Phys. **59**, 845 (1987).

¹⁸ C. W. Gardiner, Phys. Rev. A **56**, 1414 (1997), publisher: American Physical Society.

¹⁹ A. Polkovnikov, Annals of Physics **325**, 1790 (2010).

²⁰ M. Schmitt, D. Sels, S. Kehrein, and A. Polkovnikov, Phys. Rev. B **99**, 134301 (2019).

²¹ A. S. Sajna and A. Polkovnikov, arXiv:2002.05549 [cond-mat, physics:quant-ph] (2020), arXiv: 2002.05549.

²² N. Read and S. Sachdev, Phys. Rev. Lett. **66**, 1773 (1991).

²³ S. Sachdev and N. Read, Int. J. Mod. Phys. B **05**, 219 (1991).

²⁴ D. M. Newns and N. Read, Advances in Physics **36**, 799 (1987), publisher: Taylor & Francis eprint: <https://doi.org/10.1080/00018738700101082>.

²⁵ I. Affleck and J. B. Marston, Phys. Rev. B **37**, 3774 (1988).

²⁶ M. Kronenwett and T. Gasenzer, Appl. Phys. B **102**, 469 (2011).

²⁷ A. V. Gorshkov, M. Hermele, V. Gurarie, C. Xu, P. S. Julienne, J. Ye, P. Zoller, E. Demler, M. D. Lukin, and A. M. Rey, Nature Phys **6**, 289 (2010).

²⁸ S. Choudhury, K. R. Islam, Y. Hou, J. A. Aman, T. C. Killian, and K. R. A. Hazzard, Phys. Rev. A **101**, 053612 (2020), publisher: American Physical Society.

²⁹ M. Moeckel and S. Kehrein, Phys. Rev. Lett. **100**, 175702 (2008), publisher: American Physical Society.

³⁰ M. Moeckel and S. Kehrein, Annals of Physics **324**, 2146 (2009).

³¹ M. Moeckel and S. Kehrein, New J. Phys. **12**, 055016 (2010), publisher: IOP Publishing.

³² M. Eckstein, M. Kollar, and P. Werner, Phys. Rev. Lett. **103**, 056403 (2009), publisher: American Physical Society.

³³ S. A. Hamerla and G. S. Uhrig, Phys. Rev. B **89**, 104301 (2014), publisher: American Physical Society.

³⁴ J. B. Marston and I. Affleck, Phys. Rev. B **39**, 11538 (1989).

³⁵ K. Ahnert and M. Mulansky, AIP Conference Proceedings **1389**, 1586 (2011), publisher: American Institute of Physics.

³⁶ C. Sanderson and R. Curtin, The Journal of Open Source Software **1**, 26 (2016).

³⁷ C. Sanderson and R. R. Curtin, in *ICMS* (2018).

³⁸ E. Schubert and M. Gertz, in *Proceedings of the 30th International Conference on Scientific and Statistical Database Management*, SSDBM '18 (Association for Computing Machinery, Bozen-Bolzano, Italy, 2018) pp. 1–12.